Homeotropic self-alignment of discotic liquid crystals for nanoporous polymer films

ACS NANO

Cite This: ACS Nano 2018, 12, 6714–6724

www.acsnano.org

ARTICLE

Homeotropic Self-Alignment of Discotic Liquid Crystals for Nanoporous Polymer Films

Jody A. M. Lugger,[†,‡] Dirk J. Mulder,[§] Subham Bhattacharjee,[†] and Rint P. Sijbesma*[,†,‡]

[†]Institute for Complex Molecular Systems, Eindhoven University of Technology, P.O. Box 513, Eindhoven, Netherlands 5600 MB

[‡]Laboratory of Supramolecular Polymer Chemistry, Department of Chemical Engineering and Chemistry, Eindhoven University of Technology, P.O. Box 513, Eindhoven, Netherlands 5600 MB

[§]Laboratory of Stimuli-Responsive Functional Materials and Devices, Department of Chemical Engineering and Chemistry, Eindhoven University of Technology, P.O. Pox 513, Eindhoven, Netherlands 5600 MB

ABSTRACT: **Nanostructured polymer films with continuous, membrane-spanning pores from polymerizable hexagonal columnar discotic liquid crystals (LCs) were fabricated. A robust alignment method was developed to obtain homeotropic alignment of columns between glass surfaces by adding a small amount of a tri(ethylene glycol) modified analogue of the mesogen as a dopant that preferentially wets glass. The homeotropic LC alignment was fixated via a photoinitiated free radical copolymerization of a high-temperature tolerant trisallyl mesogen with a divinyl ester. Removal of the hydrogen-bonded template from the aligned columns afforded a nanoporous network with pores of nearly 1 nm in diameter perpendicular to the surface, and without noticeable collapse of the nanopores. The effect of pore orientation was demonstrated by an adsorption experiment in which homeotropic film showed a threefold increase in the initial uptake rate of methylene blue compared to planarly aligned films.**

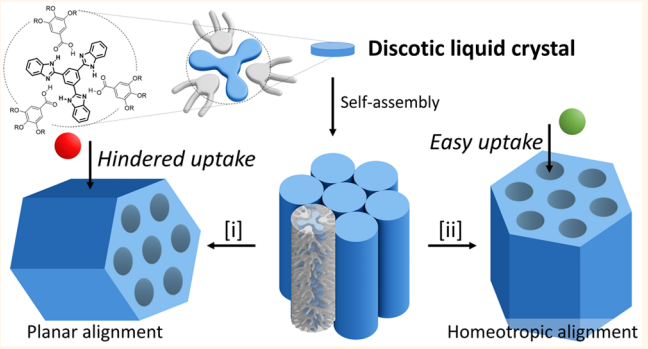

KEYWORDS: *liquid crystals, nanoporous membranes, adsorption, polymer network, homeotropic alignment*

Among the potential applications of liquid crystal (LC) based functional materials, the development of nanoporous membranes is one of the most attractive, yet challenging goals. A high density of monodisperse, nanometer-sized pores in such membranes is likely to bring about a high flux combined with enhanced size- and chemical-selectivity for high-throughput ultrafiltration.[1,2] In addition, nanoporous membranes with membrane-spanning pores will likely find their way as selective electrodes in batteries.[3−7]

For application as adsorption materials, as well as in nanoporous films, templated hydrogen-bonded discotic liquid crystals (DLCs) containing polymerizable end-groups have been used.[8,9] After polymerization of the self-assembled nanostructure and removal of the template, nanoporous materials were obtained. The benefit of DLCs is that, in contrast to nondynamic materials such as inorganic frameworks, self-assembled materials can usually be processed more easily to produce large uniform films. Efforts to develop nanostructured thin films based on polymerizable discotic liquid crystals has become a well-established research area, which has already produced a valuable basis for future applications such as membrane filtration or ion-selective layers.[10,11] However, up to now, most of the work has been performed on nonaligned nanostructured morphologies, with a few exceptions.[12,13] In order to further develop this approach toward nanoporous membranes that can potentially be used as an active layer for nano- and ultrafiltration, an effective method needs to be developed to obtain pores that span the entire thickness of the film. Bringing these materials more closely to practical applications requires homeotropic alignment of the DLCs with the column director perpendicular to the surface over large areas prior to polymerization. However, DLCs usually align in a planar fashion, with the column director parallel to the substrate because a surface that preferentially interacts with either the core or the periphery of a DLC will lead to a planar orientation of the columns (Figure 1). When there is a strong preferential surface-core interaction, it is believed that the aliphatic tails will form a strongly hydrophilic layer resulting that the next layer will again planarly align. In case of planar alignment, large area uniaxial alignment can be obtained by shearing the samples in the LC-phase. DLCs can also be aligned in a planar fashion by the help of, e.g., confined geometries such as microchannels or by the controlled casting

Received: March 10, 2018
Accepted: July 5, 2018
Published: July 5, 2018

DOI: 10.1021/acsnano.8b01822
ACS Nano 2018, 12, 6714–6724

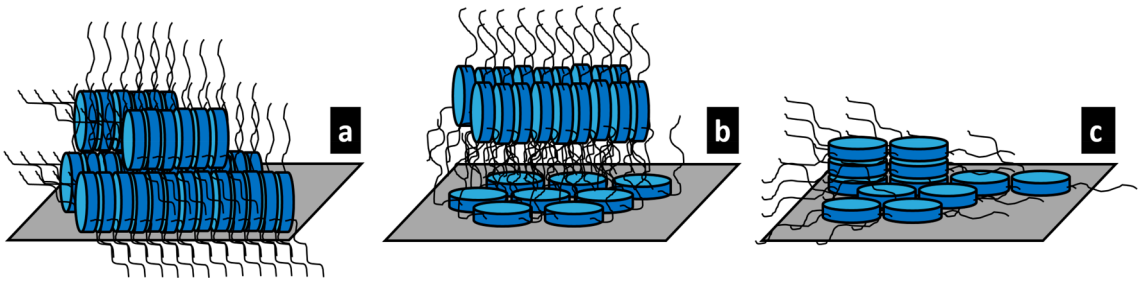

Figure 1. (a) Planar alignment is obtained when the peripheral alkyl chains have a stronger interaction with the surface than the cores. (b) When the cores of the molecules have the stronger interaction, they cover as much of the surface as possible, and force the alkyl chains to point up. This creates an apolar surface that leads to a planar alignment of the following layers. (c) Only by tuning the interfacial energy to match the entire discotic LC, a homeotropic alignment can be obtained.

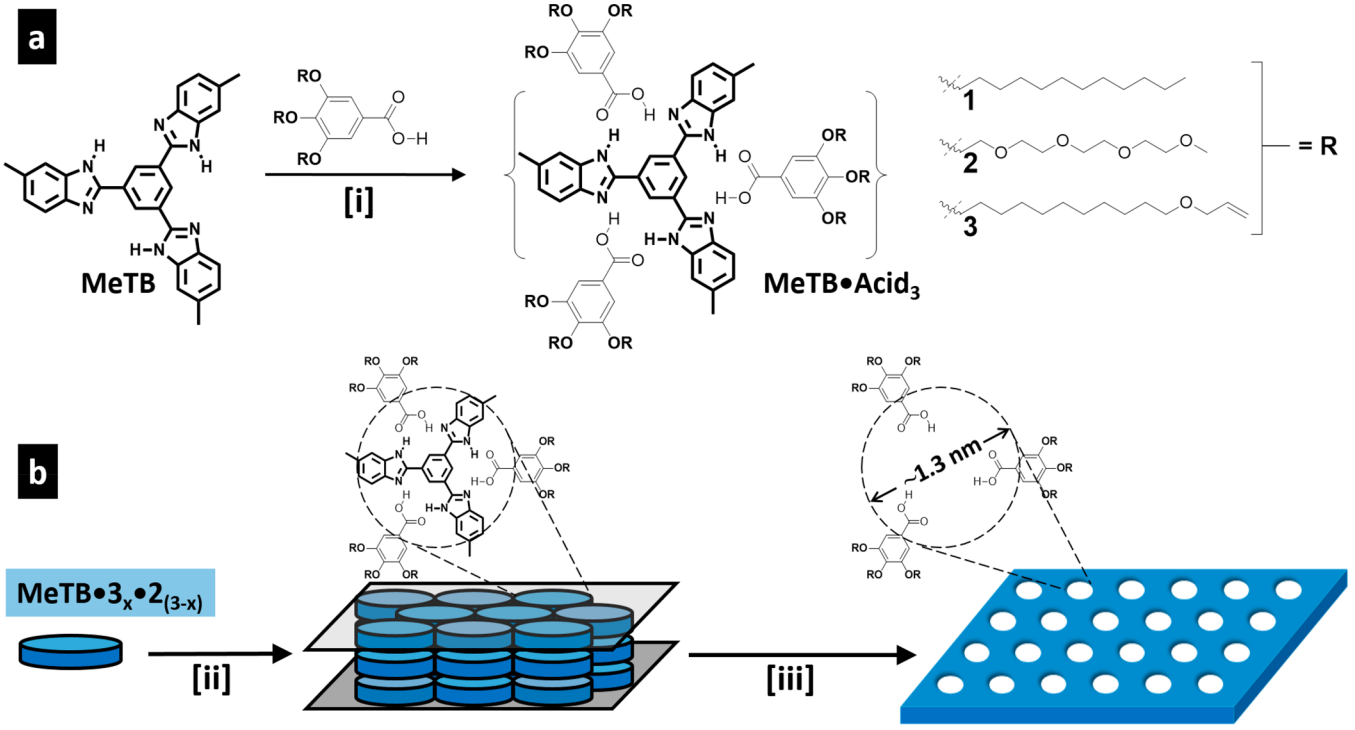

Figure 2. (a) Molecular representation of triply hydrogen-bonded discotic liquid crystals based on tris-4-methyl-benzimidazolyl benzene (MeTB) and alkylated gallic acids. (i) Self-assembly of the AB_3 hydrogen-bonded discotic liquid crystal. (b) Homeotropic alignment of the MeTB·$Acid_3$ complex by mixing in dopant 2. (ii) Homeotropic alignment of discotic LC phase between glass slides by cooling down from the isotropic phase. (iii) Fixation of the LC its columnar morphology using photoinitiated radical polymerization, followed by formation of nanopores by template removal.

from solution.[14,15] Unfortunately, after polymerization and template removal, such films will have low transport rates because the pores do not span the membrane.

Obtaining homeotropic alignment in thin films of DLCs, however, is more challenging than obtaining planar alignment, and much effort has been devoted to this goal.[16−18] The use of external fields to induce a uniform homeotropic alignment has been widely explored, e.g., electric field alignment,[19] using circularly polarized IR irradiation to control the alignment,[20] or by applying a rotating magnetic field while slowly cooling down from the isotropic phase.[21] The most common method to induce homeotropic alignment is by tuning the surface energy of the substrate, e.g. by covering a substrate with a sacrificial polymer layer that has the proper interfacial energy (Figure 1c).[22] When self-alignment of the DLC is homeotropic, large aligned areas can be obtained by the use of zone-casting.[11] The potential of using self-alignment is reflected by the observation that changing the surface energy of triphenylenes by fluorination, leads to homeotropic alignment on glass substrates compared to planar alignment in case of the fully aliphatic homologues.[23] Additionally, the interfacial energy between a nematic LC phase and water has been tuned by the addition of an amphiphilic dopant to the LC phase, which partitions to the interface, and is replenished from the bulk.[24] Inspired by this work, we sought to identify surface-active dopants that could play a similar role at the DLC−glass interface.

In the present work, homeotropically aligned DLC films are obtained by modifying the surface energy of the LC phase with a PEG derivative of the mesogen as a dopant. This alignment methodology is applied to a reactive mesogen, from which homeotropically aligned DLC based nanoporous polymer films with 1.3 nm membrane-spanning pores are prepared (Figure 2). For fixation of the homeotropic LC films, a high-

DOI: 10.1021/acsnano.8b01822
ACS Nano 2018, 12, 6714−6724

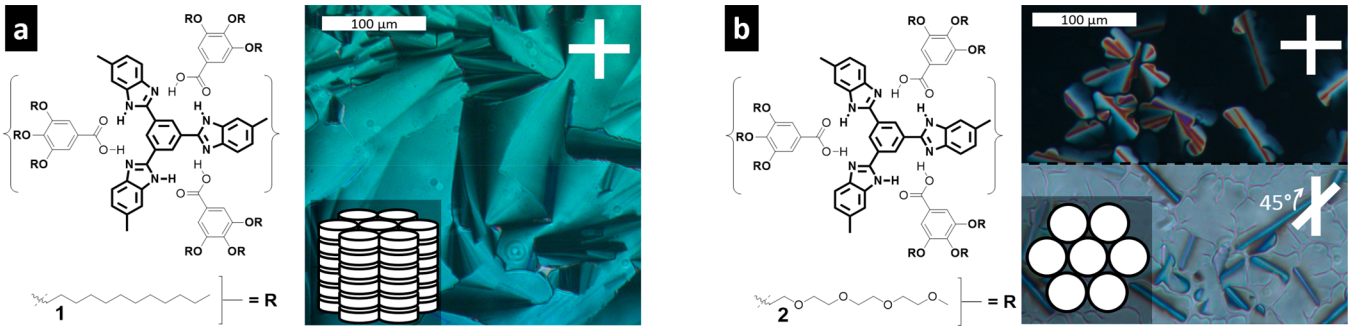

Figure 3. Illustration of switched LC alignment when using polar fatty acid. (a) POM image of a multidomain planar aligned LC texture is shown belonging to the complex MeTB·1_3. (b) POM image of the partial homeotropic texture of MeTB·2_3. Used gap size was 6 μm, and cooling speed was 2.0 °C/min from isotropic phase between glass substrates.

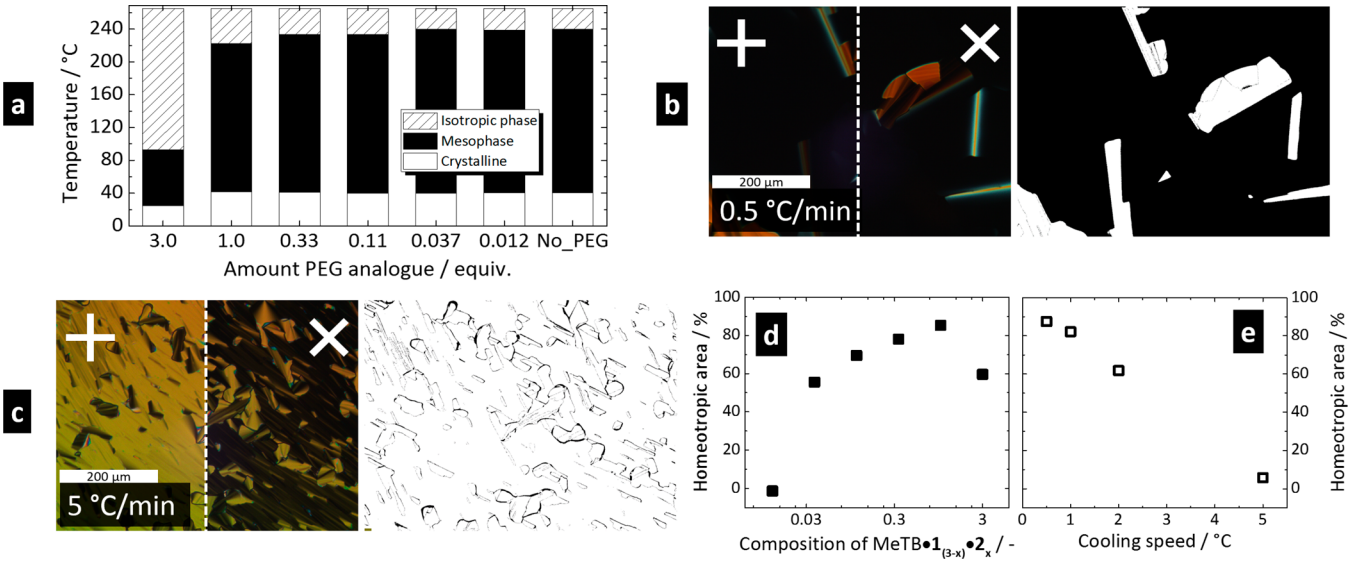

Figure 4. Inducing homeotropic alignment by doping MeTB·1_3 with hydrophilic acid 2. (a) Phase transition temperatures of different ratios of 1 and 2 mixed in the complex MeTB·$1_{(3-x)}$·2_x. (b) POM micrographs, including binarized overlay, of MeTB·1_3 cooled down from isotropic phase (0.5 °C/min) on a glass substrate coated with 2. (c) A similar analysis for 5 °C/min. (d) Homeotropic area fraction of MeTB·$1_{(3-x)}$·2_x mixtures at a cooling rate of 5 °C/min. (e) Homeotropic area fraction of MeTB·1_3 as a function of cooling speed, corresponds to shown POM images (b,c). The glass substrate was coated with a 1 wt % solution of 2, thickness < 10 nm.

temperature compatible copolymerization method of allyl ethers with vinyl esters is used.

As the basis for the current work, a previously reported hydrogen-bonded LC complex of a methylated *N*-heterocyclic template tris-4-methyl-benzimidazolyl benzene (MeTB) is used, which binds three organic acids to form a hydrogen-bonded DLC.[25−27]

RESULTS AND DISCUSSION

Homeotropic Alignment of MeTB·Acid$_3$ Complexes. The 1:3 LC complexes were formed by first dissolving the MeTB template and the gallic acid derivative in a MeOH/$CHCl_3$ mixture (1:4 v/v), followed by solvent removal. In polarized optical microscopy (POM), the 1:3 complex of aliphatic acid **1** and MeTB (MeTB·$\mathbf{1}_3$) exhibited fan-shaped domains after cooling down from the isotropic phase, typical for random planar alignment (Figure 3a). In contrast, the 1:3 complex with hydrophilic tri(ethylene glycol) analogue **2**, MeTB·$\mathbf{2}_3$, had birefringent planar as well as optically isotropic homeotropic domains. The grain boundaries of the homeotropic domains are highlighted under 45° crossed polarizers (Figure 3b). Apparently, the switch from apolar−hydrophobic to polar−hydrophilic tails switched the mode of self-alignment for the LCs.

However, for membrane applications, the use of hydrophilic oligo(ethylene glycol) containing components must be minimized since they will cause swelling of the membrane in water changing the morphology. Therefore, the efficacy of small amounts of hydrophilic acid **2** to induce homeotropic alignment of MeTB in mixtures with hydrophobic **1** was investigated.

Figure 4 shows the orientation of thin films of mixtures with intermediate composition, MeTB·$\mathbf{1}_{(3-x)}$·$\mathbf{2}_x$, where x stands for the equivalents of **2** in the complex. Analysis of the thermal phase transitions of the mixtures with differential scanning calorimetry (DSC) reveals that MeTB·$\mathbf{2}_3$ has a low clearing temperature of ∼80 °C while the mixtures (MeTB·$\mathbf{1}_{(3-x)}$·$\mathbf{2}_x$) had a clearing temperature close to that of MeTB·$\mathbf{1}_3$ (Figure 4a). Doping the complex with 1 equiv of **2** decreased the isotropization temperature by ∼20 °C from 240 to 223 °C. The efficacy of inducing homeotropic alignment by doping with **2** was determined as follows: 6 μm thick layers of the appropriate MeTB·$\mathbf{1}_{(3-x)}$·$\mathbf{2}_x$ mixture were put between glass coverslips and were cooled from the isotropic melt at 2 °C/

DOI: 10.1021/acsnano.8b01822
ACS Nano 2018, 12, 6714−6724

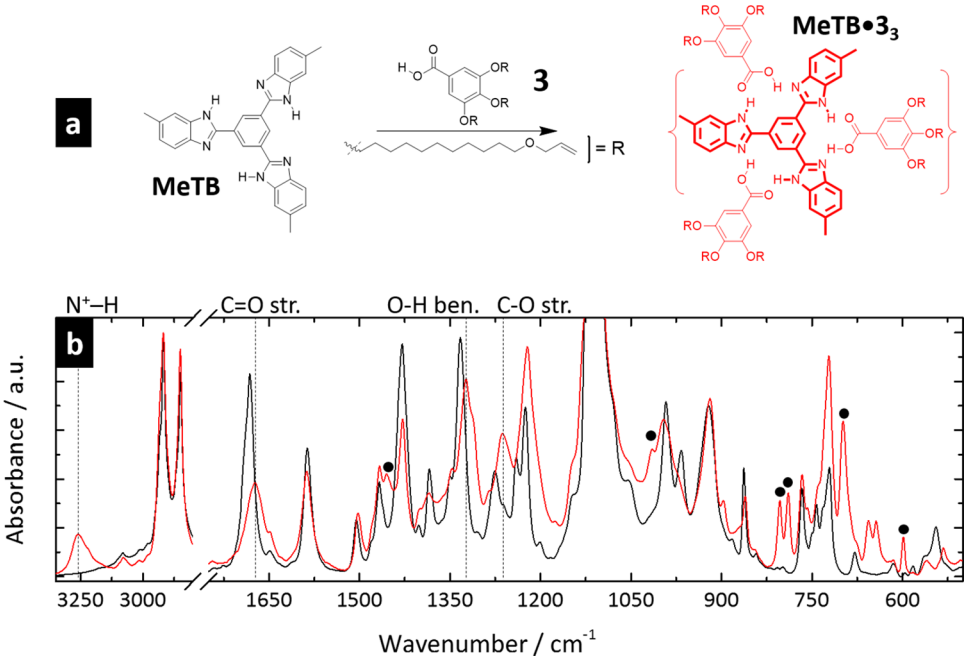

Figure 5. (a) Self-assembly of MeTB·3$_3$. (b) ATR-IR spectra of 3 and MeTB·3$_3$. Black dots indicate template specific vibrations.

min until a fully developed LC texture was observed at approximately 200 °C. The imaged field was directly used without scanning for optimal images. The area fraction of homeotropic domains was determined by overlaying two binarized optical micrographs, each with 90° crossed polarizers, the second image with both polarizers rotated by 45° relative to the first micrograph (Figure 4b,c). In such an overlaid representation, homeotropic domains show up as black.[19,23,28−30] The area fraction of homeotropic domains, a measure for the degree of homeotropic alignment, was determined twice and the average is plotted as a function of the level of doping with **2** (Figure 4d). The addition of **2** to the mixture induced homeotropic alignment at slow cooling rates up to 2 °C/min. The homeotropic area fraction was dominant when the MeTB·**1**$_{(3-x)}$·**2**$_x$ complex contained at least 0.1 equiv of **2**. Below 0.1 equiv, the homeotropic area quickly drops (Figure 4d). When a higher cooling rate of 5 °C was used, the required level of doping for predominantly homeotropic alignment increased to 0.3 equiv of **2**. A predominantly homeotropic sample was also obtained when a low concentration of **2**, 0.037 equiv., was combined with an extremely low cooling rate of 0.1 °C/min. Hence, a small amount of **2** is sufficient to obtain homeotropic samples.

The effect of hydrophilic **2** on alignment is most probably induced by preferential wetting of the glass interface. Upon cooling, the temperature gradient across the device initiates nucleation of homeotropic domains at the top surface cover, the nuclei are likely to grow further toward the bottom glass plate, thus creating homeotropically aligned LC columns from top to bottom. Increasing the content of **2** promotes the formation of homeotropic domains caused by increased partitioning of **2** to the glass surface where the domains nucleate. When the glass surface was spin-coated with a 1 wt % aqueous solution of **2**, a thin layer of less than 10 nm thick was formed, and the amount of dopant required to obtain homeotropic alignment could be further reduced to less than 0.1 wt % for a 20 μm thick LC layer (Figure 4b,c,e).

By lowering the cooling speed, the quality of alignment increased considerably: a 95% homeotropic sample was obtained with a cooling rate of 0.2 °C/min (Figure 4e). The two corresponding POM analysis are shown in Figure 4b,c. Treatment of the glass surface with trichlorododecylsilane gave full loss of the alignment effect of doping with **2**, supporting the proposed preferential wetting mechanism.

Homeotropically Aligned Polymer Films. Because of the alignment efficacy and possibility to fixate the morphology by photopolymerizing the allylic moieties, MeTB·**3**$_3$ was selected as monomer for the fabrication of a nanoporous film (Figure 2a). As expected, MeTB·**3**$_3$ showed similar behavior as MeTB·**1**$_3$, the 1:3 complex with **3** aligned homeotropically when doped with **2**. The LC complexes were formed by dissolving the components in MeOH/$CHCl_3$ (1:4 v/v) followed by drop-casting on a glass substrate. MeTB·**3**$_3$ displayed a similar fan-shaped texture as MeTB·**1**$_3$, the presence of a hexagonal columnar (Col_{hex}) phase in both cases was confirmed with X-ray diffraction (MeTB·**1**$_3$/$d_{(100)}$ = 3.16 nm vs MeTB·**3**$_3$/$d_{(100)}$ = 3.19 nm). The transition temperatures could not be determined precisely with DSC since oxidative polymerization set in before the clearing temperature was reached. The phase transition temperatures were therefore determined with POM, the following phase sequence was observed during heating: K−[50 °C]−Col_{hex}−[210 °C]−I. Formation of a 1:3 complex was further confirmed by ATR FT-infrared spectroscopy (ATR-IR), a number of differences were observed between the ATR-IR spectra of pure **3** and MeTB·**3**$_3$ (Figure 5). In the spectrum of the complex, a broad signal from the N$^+$−H vibrational band at 3259 cm^{-1} was observed, indicating a strong (ionic-like) hydrogen-bonded interaction between MeTB and **3**. The red-shift of the acid's C═O stretch vibration from 1682 to 1673 cm^{-1}, the C−O stretch from 1275 to 1261 cm^{-1}, and the O−H bending frequency from 1333 to 1322 cm^{-1} upon mixing with MeTB further confirmed the formation of a hydrogen-bonded complex. The additional vibrations observed at 1450 and

DOI: 10.1021/acsnano.8b01822
ACS Nano 2018, 12, 6714−6724

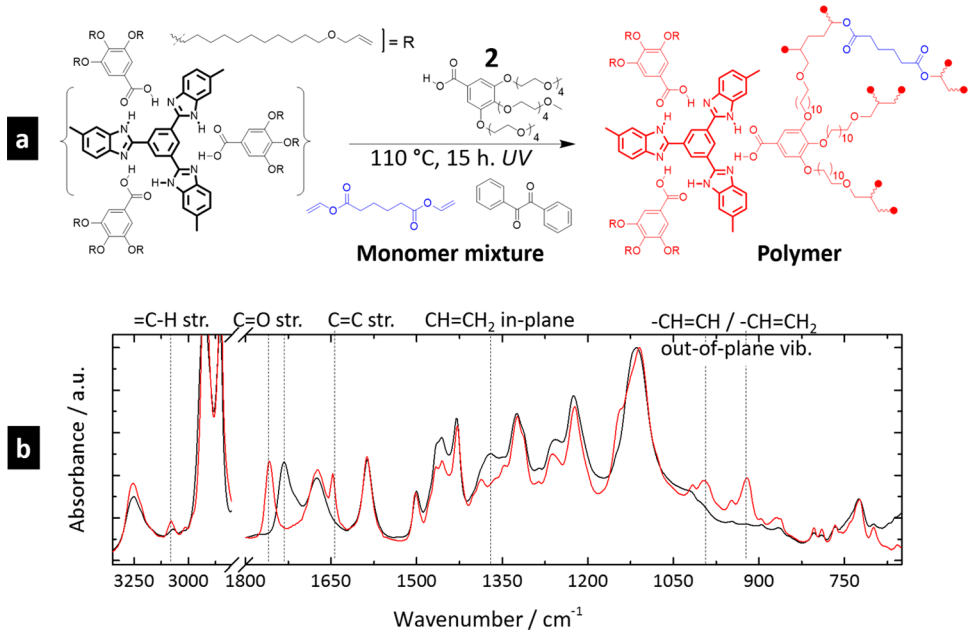

Figure 6. Fixation of Col_{hex} morphology via photoinitiated free radical polymerization. (a) Reaction scheme of polymerization. (b) IR transmission spectra of the monomer mixture (black) and resultant polymer network (red).

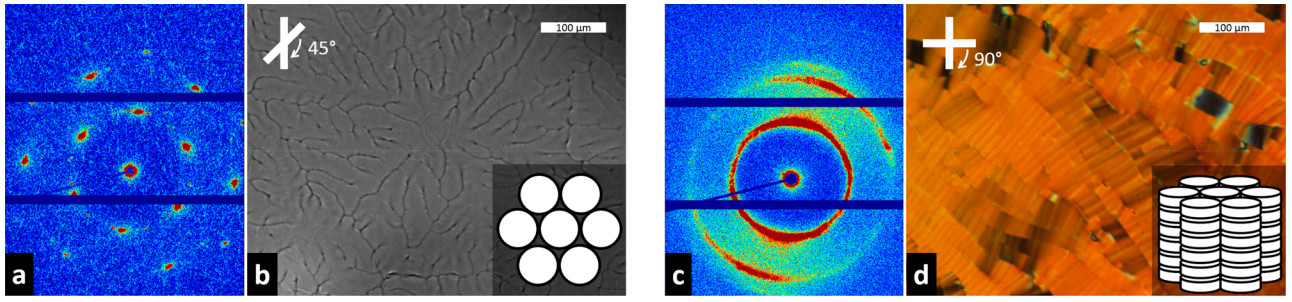

Figure 7. Nanostructured films of polymerized MeTB·3_3 in homeotropic and planar alignment. (a) 2D X-ray diffractogram of a homeotropic Col_{hex} ordered polymer network. (b) POM micrograph (with 45° crossed polarizers to highlight the grain boundaries) showing a dendritic morphology. (c) 2D X-ray diffractogram of a sample with planar alignment obtained by shearing before polymerization. (d) POM micrograph showing a multidomain planar alignment. Gap size was 20 μm, cooling speed 2.0 °C/min.

800 cm^{-1} were assigned as template specific ring-stretching and ring-bending frequencies.

Since allyl ethers do not readily form homopolymers by radical polymerization, MeTB·3_3 was polymerized in the presence of divinyl adipate, known to copolymerize with allyl ethers.[31,32] 20 wt % of divinyl adipate as a comonomer (2.7 equiv) was readily taken up by MeTB·3_3, with a 10 °C decrease in clearing temperature but without any noticeable changes of the LC texture under POM or in the infrared spectrum. Avoiding exposure to oxygen prevented the oxidative homopolymerization of **3**, which would result in early polymerization with low retention of the order. Copolymerization with divinyl adipate also improved the mechanical properties; homopolymerization of **3** gave very brittle films, presumably due to the low degree of polymerization.[33]

Aligning the LC phase by slowly cooling from the isotropic state requires that the mixture is able to withstand temperatures up to the isotropization temperature of ∼210 °C. Allyl ethers are stable when heated in an inert atmosphere. However, thermally stable photoinitiators are limited in number, but benzil proved to be a suitable candidate. When monomer mixtures containing 2 wt % benzil and comonomer were heated to the isotropization temperature of ∼195 °C, no polymerization took place, but when irradiated with UV light at 100 °C polymer films of good quality were obtained without noticeable thermal degradation. Furthermore, the alignment efficacy of the mixture was not affected by the addition of 20 wt % of divinyl adipate, 2 wt % benzil, and 5 wt % of **2**, although the clearing point decreased by approximately 15 °C.

Homeotropic alignment of the monomer mixture was achieved by placing the material between two glass slides, spaced 6−20 μm apart, followed by cooling from the isotropic liquid. High cooling rates of 2−5 °C/min could be used when 0.2 equiv of dopant **2** was present. The relatively high amount of **2** allowed the preparation of homeotropic films of up to 20 μm thickness. The samples were polymerized by irradiating overnight with an EXFO photosource equipped with a collimator, which afforded the desired homeotropically aligned nanostructured polymer films. The films were easily peeled off from the glass substrates.

Monomer conversion of the polymer films was analyzed using transmission infrared spectroscopy instead of ATR-IR to make sure that the whole film thickness was sampled. The

DOI: 10.1021/acsnano.8b01822
ACS Nano 2018, 12, 6714−6724

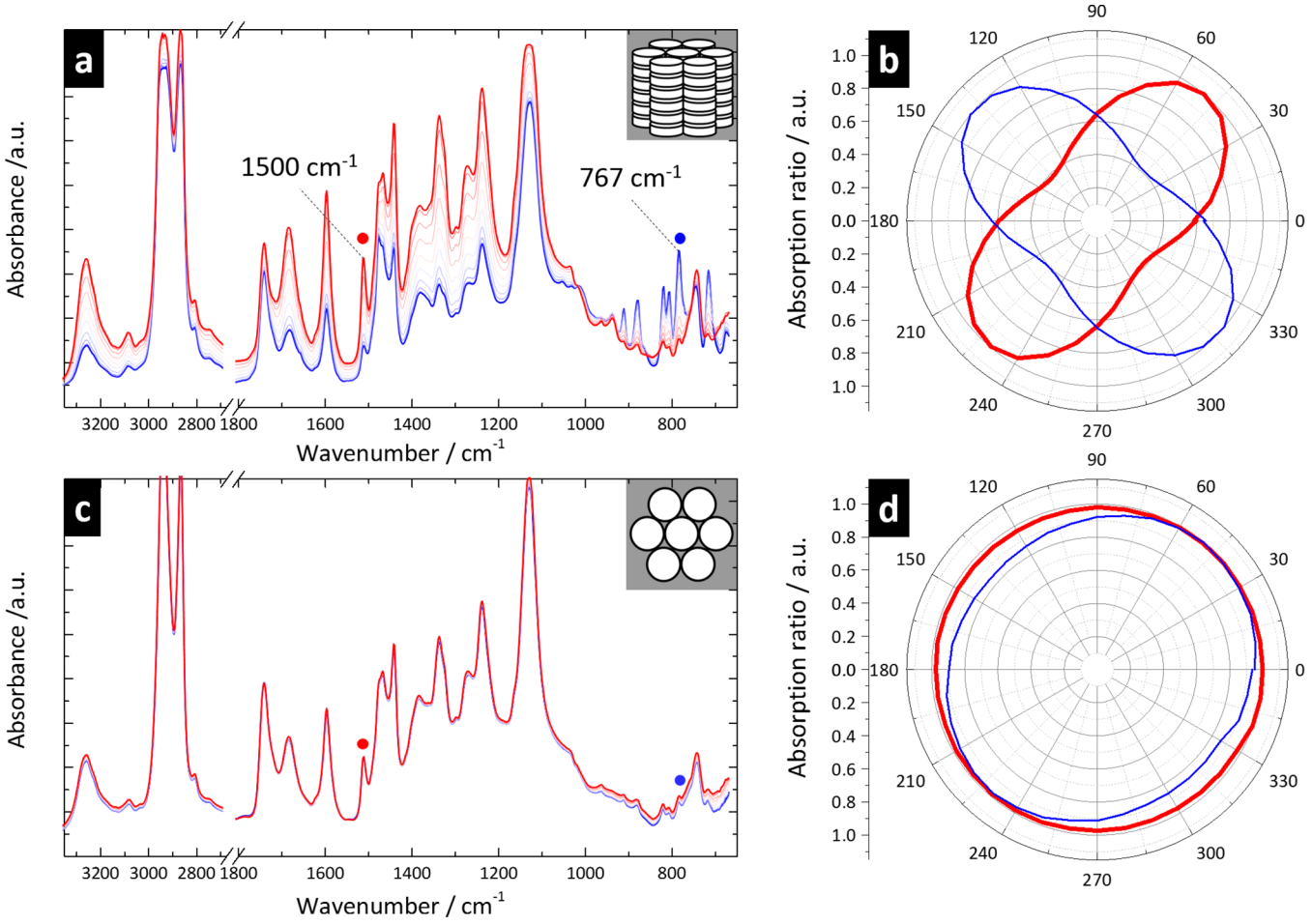

Figure 8. Polarized transmission IR spectroscopy on polymer films with homeotropic and planar alignment. (a) Stacked IR spectra of polymer with planar alignment, a range of 0−90° is shown in steps of 10°. (c) Stacked IR spectra of homeotropically aligned polymer films, a range of 0−90° is shown in steps of 10°. (b,d) Azimuthal plot of two absorption peaks, 1500 and 767 cm^{-1}, for both alignments.

polymerization of the monomers was confirmed by the disappearance of the C═C vibrational band at 1648 cm^{-1} and the ═CH and $═CH_2$ out of plane vibrations in the 800−900 cm^{-1} region (Figure 6). Furthermore, a shift of the divinyl adipate carbonyl vibration band was observed from 1758 to 1731 cm^{-1} confirming the copolymerization of the vinylic comonomer. Noteworthy is that the polymerization method did not appear to interfere with the complexation since the major absorption frequencies of MeTB·3_3 did not change. The formation of a cross-linked network was further supported by the observation that the resulting polymer was insoluble in $CHCl_3$ and DMSO.

In Figure 7a,b, a polarized optical micrograph with 45° crossed polarizers is shown together with the medium-angle 2D X-ray diffraction pattern of the homeotropically aligned polymer sample. The dendritic LC texture observed by POM is indicative of a homeotropic alignment, with only the grain boundaries being visible. Decreasing the X-ray beam size to <1000 μm^2 allowed us to selectively probe a monodomain. The 2D diffractogram showed the typical hexagonally arranged diffraction spots. With sufficient X-ray irradiation time, higher order diffraction peaks became also visible. In addition to the $d_{(100)}$ and the $d_{(110)}$ reflections at a mutual angle of 30°, the $d_{(200)}$ reflection became apparent, indicating the high degree of order within the domain. As expected, in the wide-angle X-ray diffractogram, no interdisk distance, $d_{(001)}$, was noticed for this particular alignment (data not shown). The 1D medium-angle X-ray diffractogram of the homeotropically aligned film is shown in Figure 10c.

Multidomain planar alignment was obtained by shearing the same LC mixture as used for the homeotropic sample at 100 °C between glass slides spaced 20 μm apart while monitoring the alignment using POM (Figure 7c,d). After alignment, the sample was polymerized using the same procedure as was used for the homeotropic sample. Rotating the polymerized LC film under crossed polarizers showed an alternation of bright and dark states every 45° confirming the planar alignment. The X-ray diffractogram of the film showed broadening of the diffraction peaks, which indicates imperfect alignment and the existence of multiple domains. In contrast to the homeotropic sample, the interdisk reflection was observed in the wide-angle X-ray diffractogram of the film with planar alignment (data not shown).

The two different alignments of the columnar mesophase were further studied with transmission IR and vibrational linear dichroism (Figure 8).[34] The individual IR spectra for both alignments are plotted at different azimuthal angles, with a range of 0−90° in steps of 10° (Figure 8a,c). For the sample with a planar alignment, clear dichroism is evident from the stacked spectra (Figure 8a). The molecular vibrational bands originating from the rigid core (in the fingerprint region) display a high negative anisotropy, while the N^+−H stretch of

DOI: 10.1021/acsnano.8b01822
ACS Nano 2018, 12, 6714−6724

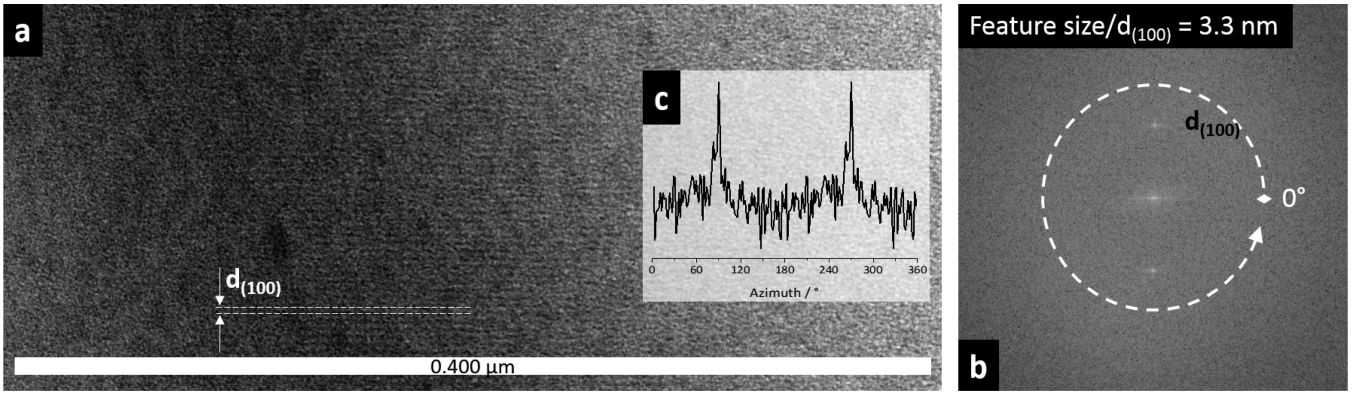

Figure 9. (a) TEM image of a planarly aligned film. (b) Fourier transform of the full image. (c) Azimuthal integration of the Fourier transform following the white dashed line.

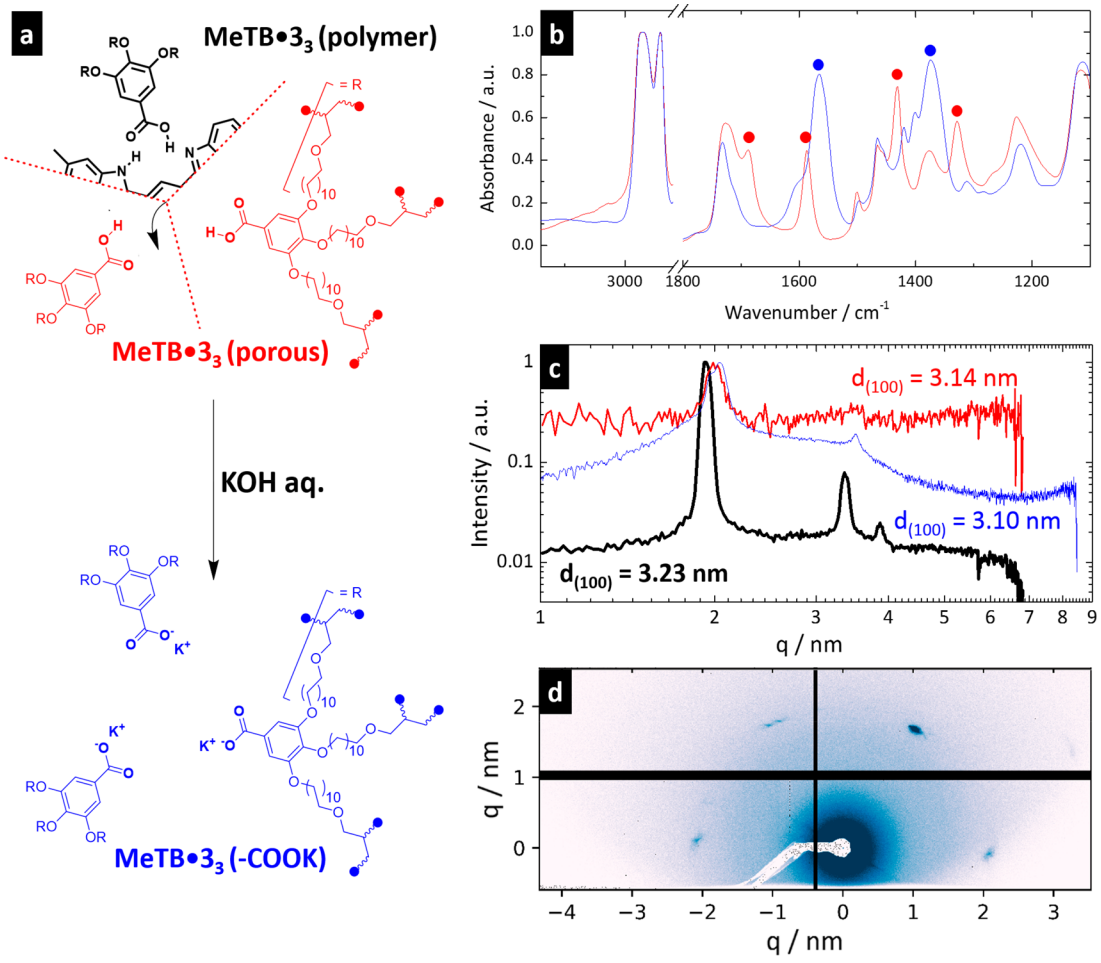

Figure 10. (a) Inducing porosity in a homeotropically aligned nanostructured polymer of MeTB·3_3 by washing out the template molecule. In a second step the −COOH interior is converted to −COOK. (b) Transmission IR spectra of MeTB·3_3 after template removal and the corresponding potassium salt. (c) X-ray diffractograms before and after template removal. (d) 2D X-ray diffractogram of the corresponding −COOK lined porous polymer.

MeTB·3_3 at 3250 cm^{-1} and the C═O stretch at 1675 cm^{-1}, had a high positive anisotropy. The orthogonal anisotropy for some of the core vibrations arises from the difference in the orientation of the IR transition moments of the respective moieties. The vibrations assigned to the aliphatic corona, e.g., 1732 cm^{-1} of the ester moiety of incorporated divinyl adipate and 725 cm^{-1} of the aliphatic backbone, are almost fully isotropic.

In contrast, the azimuthal scan of the homeotropically aligned polymer film did not show any anisotropy, indicating vertical alignment of the columns. Noteworthy, absorption of the aromatic out-of-plane vibrations is substantially lowered for the homeotropic sample. Because the columns are aligned vertical, the out-of-plane vibrations are orthogonal to the polarization vector of the incoming infrared beam. Additionally, the polar plots are shown for both alignments (Figure

DOI: 10.1021/acsnano.8b01822
ACS Nano 2018, 12, 6714−6724

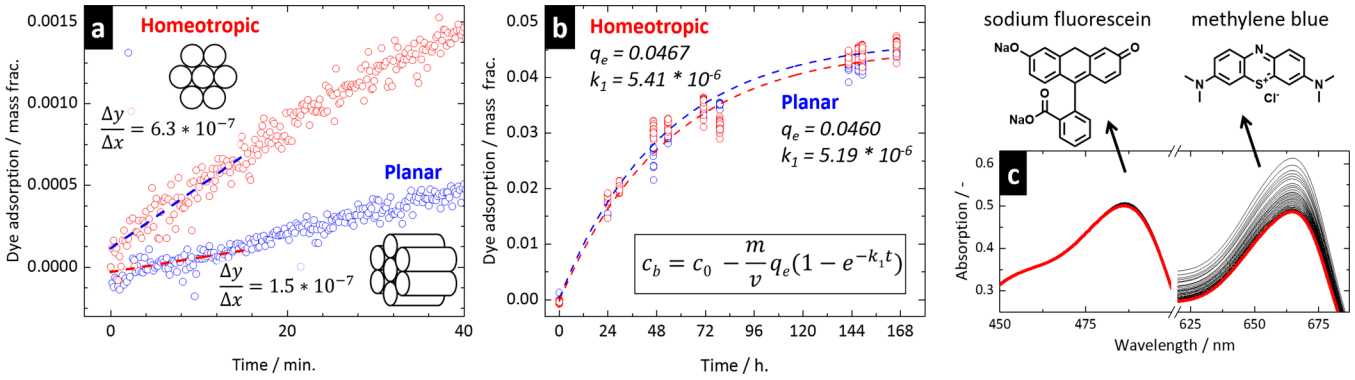

Figure 11. Methylene blue uptake over time (short time-scale) (a) for the planar and homeotropic films and (b) for a long time-scale. (c) Selective uptake of methylene blue in a competitive experiment between methylene blue and sodium fluorescein.

8b,d), with the two absorption frequencies with the most profound dichroic ratios, 1500 cm^{-1} (characteristic for aromatic C═C bending) and 767 cm^{-1} (a characteristic peak for **3** as well as MeTB), were plotted as a function of the azimuth. A high dichroic ratio was observed for the sample with planar alignment, showing C_2-symmetry (Figure 8b). For the homeotropic sample, the dichroic ratio was minimal over 360° (Figure 8d), the observed fluctuation is attributed to the limited quality of the polarizer.

The columnar order was also visualized with transmission electron microscopy (TEM) using RuO_4 stained side cuts from 6 μm thick samples embedded in epoxy resin. The obtained image suggests that the direction of the columns in the planar nonporous sample is apparently perpendicular to the shearing direction of the film (Figure 9a), which is in contrast with other examples.[35−38] Furthermore, the image shows a persistence length of the columns in the micrometer range. Calculating the Fourier transform of the image (Figure 9b), shows a repeating distance of 3.3 nm orthogonal to the columnar director, which corresponds to the $d_{(100)}$ distance of 3.23 nm as determined by X-ray diffraction. Azimuthal integration of the Fourier transformed image from a stained nonporous sample (Figure 9c) revealed two maxima, spaced 180° apart. The preparation of high-quality TEM samples is extremely challenging; unfortunately, only side cuts of the planarly aligned samples were successfully obtained.

Nanoporous thin films were produced by removing the template from the polymer network with a solution of conc. HCl (4 wt %) in DMSO at 75 °C for 16 h (Figure 10a). Transmission IR spectroscopy confirmed complete removal of the template throughout the whole film thickness. Notice the disappearance of the N^+−H stretch vibration at 3250 cm^{-1} and a blue-shift of the C═O stretch vibration to a higher wavenumber, from 1675 to 1690 cm^{-1}; comparable to pure **3** (Figure 10b). Accessibility of the acid moieties was verified by converting the free acids to the corresponding potassium salt by treating the nanoporous network with 0.04 M KOH solution in 1:1 water/THF at RT for 3 h. Full conversion of the free acids to the potassium salt was deduced from IR spectroscopy, which showed the absence of the free acid absorption band at 1690 cm^{-1} and appearance of an absorption band at 1570 and 1375 cm^{-1} belonging to the potassium salt (Figure 10b). Most importantly, XRD showed that after removing the template the hexagonal morphology was retained in the nanoporous polymer (Figure 10c), a minor 3% shrinkage of the hexagonal lattice parameter was measured after template removal. Using a synchrotron X-ray source, it was verified that the homeotropic alignment was preserved in the porous polymer (Figure 10c,d). These last observations are crucial since the work of Osuji et al. shows that simpler polymerized acids collapse after removal of the template.[12]

From the lattice parameter of the nanostructured polymer network (a = 3.73 nm) combined with the molecular weight of the template (M_w = 468.56 g/mol) and the molecular weight of the unit cell (M_w = 3591 g/mol), the pore diameter was estimated to be 1.3 nm, which corresponds to a porosity of approximately 13%. In addition, it is believed that non-polymerizable dopant **2** was also removed to a great extent, if not fully, decreasing the overall material density without effecting the material its selectivity. The latter is governed by the smallest pore diameter.

A competitive adsorption experiment (1.5 mL, 10 μM, 0.005 equiv of dye, 2 h) between positively charged methylene blue and negatively charged sodium fluorescein showed that the nanoporous film with −COOK lined pores (3.1 mg, M_w = 3188 g/mol) selectively adsorbed methylene blue into the negatively charged pores while leaving the sodium fluorescein concentration unaffected (Figure 11c). Additionally, the difference between homeotropic and planar films was demonstrated by adsorbing methylene blue from solution (Figure 11). The aligned nanoporous films of approximately 0.1 mg (20 μm thick) with −COOK lined pores were exposed to methylene blue solution (2.0 mL, 52 μM, 1 equiv of dye), the concentration of dye was monitored over time by measuring the absorbance at 588 nm spectrophotometrically. From the decrease in absorption, the methylene blue adsorption was calculated using Lambert−Beer's law ($\varepsilon_{588\ nm}$ = 20767 M^{-1}·cm, H_2O), expressed as the mass fraction q_e. The initial uptake of the films, the first 15 min, showed that the homeotropically aligned film adsorbed methylene blue 3−4 times faster than the film with planar alignment (Figure 11a). However, both the uptake speed and equilibrium adsorption of both films were similar during uptake over a longer time (Figure 11b).

Fitting the obtained concentration profile to a pseudo-first order reaction limited adsorption model gave a good quantitative description of the data (Figure 11b).[39−41] From the obtained fitted parameters (k_1, q_e) using a least-squares optimization method, it can be seen that on the long scale both films have taken up the same amount of dye ($q_e \sim$ 4.6 mg/g) with a similar rate coefficient k_1. Hence, in the steady-state, both films behave the same, meaning that the resistance for dye

DOI: 10.1021/acsnano.8b01822
ACS Nano 2018, 12, 6714−6724

uptake on longer time scales lies in the film itself and is not governed by pore entry. The better accessibility of pore ends in the homeotropically aligned sample likely caused the initial fast adsorption.

CONCLUSIONS

The self-assembly properties of discotic liquid crystals have successfully been harnessed to prepare homogeneous homeotropically aligned nanostructured polymer networks. A photoinitiated free radical polymerization method compatible with the high temperatures needed for alignment was developed. This method consisted of copolymerizing the tris-allylic LC monomers with a vinyl ester as comonomer with a thermally stable initiator.

Homeotropic, face-on alignment was induced by addition of a hydrophilic analogue of the monomer as a dopant. Samples with planar alignment were obtained by unidirectionally shearing the LC, with the same composition, prior to fixation. Removal of the hydrogen-bonded template yielded a nanoporous polymer network with membrane-spanning near-1 nm pores. The presence of free carboxylic acid groups was illustrated by conversion to the corresponding potassium salt. The initial uptake of methylene blue was 3−4 times faster in homeotropically aligned films than in planar samples, while at longer times both materials have similar uptake speed and equilibrium.

The method to prepare nanoporous membranes with near-1 nm pores from polymerizable DLCs offers ample opportunities to develop fully functional materials. The strategy presented here can be easily extended toward the fabrication of functioning active layers for membrane technologies. The strategy of tuning the LC-interfacial energy can be generally applied under the condition that the additive is miscible and does not interfere with the LC self-assembly.

EXPERIMENTAL SECTION

General. Commercially purchased chemicals were used without further purification. MeTB and tri(ethylene glycol) analogue **2** were prepared according to their reported synthesis.[26,27] Column chromatography was carried out using silica gel (0.035−0.070 mm, ca. 6 nm pore diameter). ATR FT-IR spectra were recorded at room temperature on a PerkinElmer Spectrum Two spectrometer equipped with a universal attenuated total reflectance (ATR) sampling accessory. Transmission FT-IR spectra were recorded on a Varian 670 IR spectrometer, equipped with a microscope setup. Scans were taken over a range of 4000−400 cm^{-1}, with a spectral resolution of 4 cm^{-1}, 100 scans per spectrum. Processing of the transmission FT-IR spectra was done using Varian FTS 3000 Excalibur Resolutions, version 4.0.5.009, software. NMR spectra were recorded at room temperature on a Bruker, FT-NMR spectrometer AVANCE III HD-NanoBay (400 MHz, Bruker UltraSchield magnet, BBFO Probehead, BOSS1 shim assembly) in $CDCl_3$. Chemical shifts are given in ppm with respect to tetramethylsilane (TMS, 0 ppm). Coupling constants are reported as *J*-values in Hz. MALDI-TOF-MS analysis was performed on a Bruker, speed autoflex, operated in reflectron mode with a positive voltage polarity, 500 shots. Cesium tri-iodide was used as calibration reference. α-Cyano-4-hydroxycinnamic acid (CHCA, 20 mg/mL) and *trans*-2-[3-(4-*tert*-butylphenyl)-2-methyl-2-propenylidene]malononitrile (DCTB, 30 mg/mL) were used as the matrix. Samples were prepared by mixing 1 μL (1 mg/mL) of sample 1:1 with the matrix solution, after which the mixture was spotted on the MALDI plate. It was noticed that the tris-allyl 3 polymerizes/decomposes during drying of the MALDI plate; direct insertion of the plate after spotting solved this problem. Exact molecular masses were calculated using IsoPro 3.0, MS/MS Software. POM was performed with a Jeneval microscope equipped with crossed polarizers, a Linkam THMS 600 heating stage, and a Polaroid DMC le CCD camera. DSC measurements were performed in hermetic T-zero aluminum sample pans using a TA Instruments Q2000−1037 DSC instrument equipped with a RCS90 cooling accessory. Transition temperatures and enthalpies were typically determined from the first cooling and first heating run using Universal Analysis 2000 software (TA Instruments, USA), with heating and cooling rates of 10 K/min. X-ray scattering measurements were performed on a Ganesha lab instrument equipped with a Genix-Cu ultralow divergence source producing X-ray photons with a wavelength of 0.154 nm and a flux of 1×10^8 photons s^{-1}. Diffraction patterns were collected using a Pilatus 300 K silicon pixel detector with 487 × 619 pixels of 172 μm^2 in size, placed at a sample to detector distance of 91 mm (wide angle, WAXS), or 500 mm (medium angle, MAXS). On the obtained diffraction patterns an azimuthal integration was performed, using SAXSGUI software, to calculate the intensity against the scattering vector q, where $q = (4\pi/\lambda)\sin\vartheta$ (ϑ is the angle of incidence and λ is the wavelength). The beam center and the q-range were calibrated using silver behenate ($d_{(100)}$ = 1.076 nm^{-1}; 5.839 nm), as a reference. The $d_{(300)}$ was used for calibration. Temperature was controlled with a Linkam HFSX350 heating stage and cooling unit. Measurements were performed on bulk samples sealed in 1.0 mm diameter glass capillaries, 0.01 mm wall thickness (Hilgenberg). Beam size was minimized (~30 μm in diameter) for the homeotropic sample to ensure the sampling of a monodomain. The planar sample and the monomer mixture were measured using a normal, wider, beam. Grazing-incidence small-angle scattering (GISAXS) measurements were performed at the BM26B-DUBBLE beamline at the ESRF. An X-ray wavelength of λ = 0.1 nm was used with 2 and 4 m sample-to-detector distances. GISAXS images were recorded using a solid state silicon photon counting Pilatus 1 M detector with pixel size of 172 × 172 μm and active surface dimension of 179 × 169 cm. The scattering angle scale 2θ was calibrated using the position of diffraction rings from silver behenate powder. Direct and reflected beam positions were measured directly on the detector using a 2 mm Al filter to reduce the direct beam intensity and avoid detector damage. The nominal incident angles α_i were accurately recalibrated using the measured reflected beam position and the known sample-to-detector distance. Different angles of incidence α_i ranging from 0.08° to 1.1° were used in order to allow increased penetration depth of the supported networks. Background scattering from air was subtracted to every image before further analysis. Scattering from glass substrate was not subtracted as it contributes much less than the sample to the experimentally measured GISAXS intensity. Sample preparation for transmission electron microscopy (TEM) was as follows: the thin films were embedded in an epoxy resin, EPOFIX, and cured at 70 °C, 1 h. Ultrathin sections were obtained at room temperature using a Leica Reichert-Jung Ultracut E microtome, equipped with a Diatome 45° knife, set to 60−70 nm thickness. The cross sections were transferred to a 200/400 mesh copper grid with a carbon support layer. The sections were additionally stained with RuO_4 vapor for 15 min, using a freshly prepared $RuCl_3$/hypochlorite solution.[42] The imaging was performed on a TU/e CryoTitan (FEI) is equipped with a field emission gun operating at 300 kV and with a postcolumn Gatan energy filter. Images were recorded using a 2 k × 2 k Gatan CCD camera. The LC mixtures were prepared as follows: the required amount of acid and template were measured separately; typically, 20 mg of total sample was obtained. The acid was analytically transferred to the template using 500 μL of chloroform. To ensure full dissolution of all components, 100 μL of methanol was added. The solvent was removed using a rotary evaporator, and the mixture was further dried using a vacuum pump (<1 mbar). Before testing, each sample was thoroughly mixed. The monomeric mixtures containing reactive mesogens were prepared from stock solutions: solution 1:15 μmol solution of MeTB·3_3 complex (~20 mg/mL) in 20 v/v % MeOH/$CHCl_3$, solution 2:67,5 μmol divinyl adipate, 6 μmol benzil, 9 μmol tri(ethylene glycol) analog **2**, dissolved in 20 v/v % MeOH/$CHCl_3$. The appropriate samples were prepared by mixing equal volumes of solutions 1 and 2 and drop casting the final solution on the substrate

DOI: 10.1021/acsnano.8b01822
ACS Nano 2018, 12, 6714−6724

at 50 °C (to prevent oxidative polymerization). To obtain the homeotropic alignment: after placing the cover substrate, the sample was heated to the isotropic temperature followed by cooling 2 K/min to 100 °C. For the planar aligned sample the mixture was directly heated to 100 °C, and manually sheared in one direction until an acceptable degree of alignment was achieved as was judged from the POM by the naked eye. Polymerization of the samples was done at 100 °C, irradiation time was 900 min. (15 h). Different ways of treating the glass surface, i.e., no treatment, washing with i-propanol, UV-ozone treatment, or treating with piranha solution (3:1, conc. H_2SO_4/H_2O_2 30%), had no noticeable effect on the alignment efficacy.

Synthetic Procedures. Synthesis of 3,4,5-tris((11-(allyloxy)-undecyl)oxy)benzoic acid (5): Methyl gallate (200 mg, 1.09 mmol, 1 equiv) was added to a suspension of potassium carbonate (1.5 g, 10.9 mmol, 10 equiv) in DMF (7 mL). The slurry was heated to 75 °C, for 30 min. 1-(Allyloxy)-11-bromoundecane (1 g, 1 mmol, 1 equiv), prepared using a reported procedure,[43] was dissolved in DMF (1 mL) and was slowly added to the suspension using a syringe. The slurry was stirred overnight at 75 °C, the round-bottom flask was sealed using a U-tube filled with mineral oil. The mixture was allowed to cool to room temperature, followed by filtration over a silica plug (5 g) using chloroform. Separating the methyl ester from the starting bromide tail was unsuccessful. The crude mixture was therefore directly hydrolyzed to the final acid; the crude wax was treated with the following mixture: KOH (1 g), water (2.5 mL), MeOH (7.5 mL) and THF (10 mL) for 1 h. Conversion was checked with TLC (silica, heptane/$CHCl_3$/EtOH/AcOH, 7:2.5:0.5:0.1, R_f = 0.28). The final compound **5** was isolated by column chromatography (80 g silica, heptane/$CHCl_3$/EtOH/AcOH, 7:2.5:0.3:0.1) affording 348 mg of a white wax, overall 40% yield. ^{1}H NMR (400 MHz, $CDCl_3$, 25 °C, TMS): δ = 10.47 (b, 1 H; −COOH), 7.32 (s, 2 H; Ar−H), 5.92 (tdd, $J_{(H,H)}$ = 5.6 Hz; 10.4 Hz; 17.2 Hz, 3 H; CH_2═CH−), 5.27 (dd, $J_{(H,H)}$ = 1.5 Hz; 17.2 Hz, 3 H; *cis*-CHH═CH−), 5.16 (dd, $J_{(H,H)}$ = 1.5 Hz; 10.4 Hz, 3 H; *trans*-CHH═CH−), 4.04 (t, $J_{(H,H)}$ = 6.4 Hz, 2 H; Ar−O−CH_2−), 4.02 (t, $J_{(H,H)}$ = 6.4 Hz, 4 H; Ar−O−CH_2−), 3.97 (d, $J_{(H,H)}$ = 5.6 Hz, 6 H; −O−CH_2−CH−), 3.43 (t, $J_{(H,H)}$ = 6.7 Hz, 4 H; −CH2−O−CH_2−CH−), 3.42 (t, $J_{(H,H)}$ = 6.7 Hz, 2 H; −CH_2−O−CH_2−CH−), 1.82 (p, $J_{(H,H)}$ = 6.4/7.2 Hz, 4 H; Ar−O−CH_2−CH_2−), 1.75 (p, $J_{(H,H)}$ = 6.4/7.2 Hz, 2 H; Ar−O−CH_2−CH_2−), 1.59 (p, $J_{(H,H)}$ = 6.7/7.0 Hz, 6 H; −CH_2−CH_2−O−CH_2−CH−), 1.48 (p, $J_{(H,H)}$ = 7.2 Hz, 6 H; Ar−O−$(CH_2)_2$−CH_2−), 1.29 (m, 36 H; −CH2−CH_2−CH_2−). ^{13}C NMR (101 MHz, $CDCl_3$, 25 °C, TMS): δ = 171.21, 152.84, 143.08, 135.09, 135.08, 123.77, 116.73, 116.69, 108.59, 73.53, 71.79, 70.52, 69.18, 30.32, 29.78, 29.75, 29.70, 29.67, 29.65, 29.59, 29.56, 29.54, 29.51, 29.35, 29.26, 26.23, 26.20, 26.04. MALDI/TOF-MS (500 shots, positive mode, CHCA and DCTB): calculated exact mass for $C_{49}H_{84}O_8$ = 800.617 g/mol, measured m/z = 823.60 [M + Na^+] and 839.58 [M + K^+] using CHCA, and 823.60 [M + Na^+] using DCTB. IR (ATR, 16 scans): 3080, 2918, 2850, 1682, 1586, 1505, 1467, 1430, 1383, 1332, 1275, 1239, 1226, 1124, 1111, 992, 967, 921, 863, 766, 742, 722, 679, 615, 583, 545, 492.

AUTHOR INFORMATION

Corresponding Author

*E-mail: R.P.Sijbesma@tue.nl.

ORCID

Rint P. Sijbesma: 0000-0002-8975-636X

Author Contributions

D.J.M. performed the transmission IR measurements, sample preparation for the TEM measurements, and structuring and drafting of the manuscript. R.P.S. supervised the work and revised the manuscript. S.B. measured the ion selectivity of the material. J.A.M.L. prepared the materials, performed the experiments, and wrote the manuscript.

Notes

The authors declare no competing financial interest.

ACKNOWLEDGMENTS

The research was supported by the Ministry of Education, Culture and Science of The Netherlands (Gravity Program 024.001.035) and partly financed by The Netherlands Organisation for Scientific Research (NWO), Project Number 729.002.003. This research forms part of the research program of the Dutch Polymer Institute (DPI), Project 776. The authors sincerely thank P. Bomans, A. Spoelstra, and A. Bus for their valuable help with the TEM measurements and interpretation.

REFERENCES

(1) Schenning, A. P. H. J.; Gonzalez-Lemus, Y. C.; Shishmanova, I. K.; Broer, D. J. Nanoporous Membranes Based on Liquid Crystalline Polymers. *Liq. Cryst.* **2011**, *38*, 1627−1639.

(2) Kim, W.; Nair, S. Membranes from Nanoporous 1D and 2D Materials: A Review of Opportunities, Developments, and Challenges. *Chem. Eng. Sci.* **2013**, *104*, 908−924.

(3) Perry, M. L. Expanding the Chemical Space for Redox Flow Batteries. *Science* **2015**, *349*, 1452−1452.

(4) Ye, J.; Baumgaertel, A. C.; Wang, Y. M.; Biener, J.; Biener, M. M. Structural Optimization of 3D Porous Electrodes for High-Rate Performance Lithium Ion Batteries. *ACS Nano* **2015**, *9*, 2194−2202.

(5) Deimede, V.; Elmasides, C. Separators for Lithium-Ion Batteries: A Review on the Production Processes and Recent Developments. *Energy Technology* **2015**, *3*, 453−468.

(6) Kerr, R. L.; Miller, S. A.; Shoemaker, R. K.; Elliott, B. J.; Gin, D. L. New Type of Li Ion Conductor with 3D Interconnected Nanopores *via* Polymerization of a Liquid Organic Electrolyte-Filled Lyotropic Liquid-Crystal Assembly. *J. Am. Chem. Soc.* **2009**, *131*, 15972−15973.

(7) Soberats, B.; Yoshio, M.; Ichikawa, T.; Ohno, H.; Kato, T. Zwitterionic Liquid Crystals as 1D and 3D Lithium Ion Transport Media. *J. Mater. Chem. A* **2015**, *3*, 11232−11238.

(8) Lee, H.-K.; Lee, H.; Ko, Y. H.; Chang, Y. J.; Oh, N.-K.; Zin, W.-C.; Kim, K. Synthesis of a Nanoporous Polymer with Hexagonal Channels from Supramolecular Discotic Liquid Crystals. *Angew. Chem., Int. Ed.* **2001**, *40*, 2669−2671.

(9) Bögels, G. M.; van Kuringen, H. P. C.; Shishmanova, I. K.; Voets, I. K.; Schenning, A. P. H. J.; Sijbesma, R. P. Selective Absorption of Hydrophobic Cations in Nanostructured Porous Materials from Crosslinked Hydrogen-Bonded Columnar Liquid Crystals. *Adv. Mater. Interfaces* **2015**, *2*, 1500022.

(10) Wang, G.; Garvey, C. J.; Zhao, H.; Huang, K.; Kong, L. Toward the Fabrication of Advanced Nanofiltration Membranes by Controlling Morphologies and Mesochannel Orientations of Hexagonal Lyotropic Liquid Crystals. *Membranes* **2017**, *7*, 37.

(11) Tracz, A.; Makowski, T.; Masirek, S.; Pisula, W.; Geerts, Y. H. Macroscopically Aligned Films of Discotic Phthalocyanine by Zone Casting. *Nanotechnology* **2007**, *18*, 485303.

(12) Feng, X.; Kawabata, K.; Kaufman, G.; Elimelech, M.; Osuji, C. O. Highly Selective Vertically Aligned Nanopores in Sustainably Derived Polymer Membranes by Molecular Templating. *ACS Nano* **2017**, *11*, 3911−3921.

(13) Feng, X.; Tousley, M. E.; Cowan, M. G.; Wiesenauer, B. R.; Nejati, S.; Choo, Y.; Noble, R. D.; Elimelech, M.; Gin, D. L.; Osuji, C. O. Scalable Fabrication of Polymer Membranes with Vertically Aligned 1 Nm Pores by Magnetic Field Directed Self-Assembly. *ACS Nano* **2014**, *8*, 11977−11986.

(14) Bramble, J. P.; Tate, D. J.; Revill, D. J.; Sheikh, K. H.; Henderson, J. R.; Liu, F.; Zeng, X.; Ungar, G.; Bushby, R. J.; Evans, S. D. Planar Alignment of Columnar Discotic Liquid Crystals by Isotropic Phase Dewetting on Chemically Patterned Surfaces. *Adv. Funct. Mater.* **2010**, *20*, 914−920.

(15) Tracz, A.; Jeszka, J. K.; Watson, M. D.; Pisula, W.; Müllen, K.; Pakula, T. Uniaxial Alignment of the Columnar Super-Structure of a

DOI: 10.1021/acsnano.8b01822
ACS Nano 2018, 12, 6714−6724

Hexa (Alkyl) Hexa-Peri-Hexabenzocoronene on Untreated Glass by Simple Solution Processing. *J. Am. Chem. Soc.* **2003**, *125*, 1682−1683.
(16) Wöhrle, T.; Wurzbach, I.; Kirres, J.; Kostidou, A.; Kapernaum, N.; Litterscheidt, J.; Haenle, J. C.; Staffeld, P.; Baro, A.; Giesselmann, F.; Laschat, S. Discotic Liquid Crystals. *Chem. Rev.* **2016**, *116*, 1139−1241.
(17) Kaafarani, B. R. Discotic Liquid Crystals for Opto-Electronic Applications. *Chem. Mater.* **2011**, *23*, 378−396.
(18) Charlet, E.; Grelet, E.; Brettes, P.; Bock, H.; Saadaoui, H.; Cisse, L.; Destruel, P.; Gherardi, N.; Seguy, I. Ultrathin Films of Homeotropically Aligned Columnar Liquid Crystals on Indium Tin Oxide Electrodes. *Appl. Phys. Lett.* **2008**, *92*, 024107.
(19) Sato, K.; Itoh, Y.; Aida, T. Columnarly Assembled Liquid-Crystalline Peptidic Macrocycles Unidirectionally Orientable over a Large Area by an Electric Field. *J. Am. Chem. Soc.* **2011**, *133*, 13767−13769.
(20) Monobe, H.; Awazu, K.; Shimizu, Y. Alignment Control of a Columnar Liquid Crystal for a Uniformly Homeotropic Domain Using Circularly Polarized Infrared Irradiation. *Adv. Mater.* **2006**, *18*, 607−610.
(21) Ikeda, S.; Takanishi, Y.; Ishikawa, K.; Takezoe, H. Magnetic Field Effect on the Alignment of a Discotic Liquid Crystal. *Mol. Cryst. Liq. Cryst. Sci. Technol., Sect. A* **1999**, *329*, 589−595.
(22) Pouzet, E.; Cupere, V. D.; Heintz, C.; Andreasen, J. W.; Breiby, D. W.; Nielsen, M. M.; Viville, P.; Lazzaroni, R.; Gbabode, G.; Geerts, Y. H. Homeotropic Alignment of a Discotic Liquid Crystal Induced by a Sacrificial Layer. *J. Phys. Chem. C* **2009**, *113*, 14398−14406.
(23) Terasawa, N.; Monobe, H.; Kiyohara, K.; Shimizu, Y. Strong Tendency towards Homeotropic Alignment in a Hexagonal Columnar Mesophase of Fluoroalkylated Triphenylenes. *Chem. Commun.* **2003**, 1678.
(24) Yang, Z.; Gupta, J. K.; Kishimoto, K.; Shoji, Y.; Kato, T.; Abbott, N. L. Design of Biomolecular Interfaces Using Liquid Crystals Containing Oligomeric Ethylene Glycol. *Adv. Funct. Mater.* **2010**, *20*, 2098−2106.
(25) Xiong, J.-F.; Luo, S.-H.; Huo, J.-P.; Liu, J.-Y.; Chen, S.-X.; Wang, Z.-Y. Design, Synthesis, and Characterization of 1,3,5-Tri(1H-Benzo[d]Imidazol-2-Yl)Benzene-Based Fluorescent Supramolecular Columnar Liquid Crystals with a Broad Mesomorphic Range. *J. Org. Chem.* **2014**, *79*, 8366−8373.
(26) Lugger, J. A. M.; Sijbesma, R. P. Easily Accessible Thermotropic Hydrogen-Bonded Columnar Discotic Liquid Crystals from Fatty Acid− Tris-Benzoimidazolyl Benzene Complexes. *ChemistryOpen* **2016**, *5*, 580−585.
(27) Bögels, G. M.; Lugger, J. A. M.; Goor, O. J. G. M.; Sijbesma, R. P. Size-Selective Binding of Sodium and Potassium Ions in Nanoporous Thin Films of Polymerized Liquid Crystals. *Adv. Funct. Mater.* **2016**, *26*, 8023−8030.
(28) De Cupere, V.; Tant, J.; Viville, P.; Lazzaroni, R.; Osikowicz, W.; Salaneck, W. R.; Geerts, Y. H. Effect of Interfaces on the Alignment of a Discotic Liquid−Crystalline Phthalocyanine. *Langmuir* **2006**, *22*, 7798−7806.
(29) Schweicher, G.; Gbabode, G.; Quist, F.; Debever, O.; Dumont, N.; Sergeyev, S.; Geerts, Y. H. Homeotropic and Planar Alignment of Discotic Liquid Crystals: The Role of the Columnar Mesophase. *Chem. Mater.* **2009**, *21*, 5867−5874.
(30) Wang, J.; He, Z.; Zhang, Y.; Zhao, H.; Zhang, C.; Kong, X.; Mu, L.; Liang, C. The Driving Force for Homeotropic Alignment of a Triphenylene Derivative in a Hexagonal Columnar Mesophase on Single Substrates. *Thin Solid Films* **2010**, *518*, 1973−1979.
(31) Shigetomi, Y.; Kojima, T.; Ono, N. Allylic Polymers. I. Copolymerization of Allyl Esters with Vinyl Acetate. *J. Polym. Sci., Part A: Polym. Chem.* **1990**, *28*, 3317−3325.
(32) Shigetomi, Y.; Ono, N.; Kato, H.; Oki, M. Allylic Polymers IV. The Effect of Alkyl-Substituents on Copolymerization of Allyl Alkyl Ethers with Vinyl Acetate. *Polym. J.* **1992**, *24*, 247−255.
(33) Matsumoto, A.; Kumagai, T.; Aota, H.; Kawasaki, H.; Arakawa, R. Reassessment of Free-Radical Polymerization Mechanism of Allyl Acetate Based on End-Group Determination of Resulting Oligomers by MALDI-TOF-MS Spectrometry. *Polym. J.* **2009**, *41*, 26−33.
(34) Vij, J. Advances in liquid crystals. In *Advances in Chemical Physics*;Rice, S. A., Ed.; Wiley: New York, 2000; Vol. *113*.
(35) Kang, D.-G.; Park, M.; Kim, D.-Y.; Goh, M.; Kim, N.; Jeong, K.-U. Heat Transfer Organic Materials: Robust Polymer Films with the Outstanding Thermal Conductivity Fabricated by the Photo-polymerization of Uniaxially Oriented Reactive Discogens. *ACS Appl. Mater. Interfaces* **2016**, *8*, 30492−30501.
(36) Kang, D.-G.; Kim, D.-Y.; Park, M.; Choi, Y.-J.; Im, P.; Lee, J.-H.; Kang, S.-W.; Jeong, K.-U. Hierarchical Striped Walls Constructed by the Photopolymerization of Discotic Reactive Building Blocks in the Anisotropic Liquid Crystal Solvents. *Macromolecules* **2015**, *48*, 898−907.
(37) Kim, J.; Yamasaki, N.; Hayashi, T.; Yoshida, H.; Moritake, H.; Fujii, A.; Shimizu, Y.; Ozaki, M. High-Quality Planar Alignment of Discotic Liquid Crystals Using Oscillating Shear. *Appl. Phys. Express* **2013**, *6*, 061702.
(38) Kim, N.; Wang, L.; Kim, D.-Y.; Hwang, S.-H.; Kuo, S.-W.; Lee, M.-H.; Jeong, K.-U. Macroscopically Oriented Hierarchical Structure of the Amphiphilic Tetrathiafulvalene Molecule. *Soft Matter* **2012**, *8*, 9183−9192.
(39) Yuh-Shan, H. Citation Review of Lagergren Kinetic Rate Equation on Adsorption Reactions. *Scientometrics* **2004**, *59*, 171−177.
(40) Ho, Y.-S. Review of Second-Order Models for Adsorption Systems. *J. Hazard. Mater.* **2006**, *136*, 681−689.
(41) Simonin, J.-P. On the Comparison of Pseudo-First Order and Pseudo-Second Order Rate Laws in the Modeling of Adsorption Kinetics. *Chem. Eng. J.* **2016**, *300*, 254−263.
(42) Montezinos, D.; Wells, B. G.; Burns, J. L. The Use of Ruthenium in Hypochlorite as a Stain for Polymeric Materials. *J. Polym. Sci., Polym. Lett. Ed.* **1985**, *23*, 421−425.
(43) Breed, P. G.; Ramsden, J. A.; Brown, J. M. Scope and Limitations of Ruthenium-Catalyzed Metathesis of Simple Polymer-Bound Alkenes. *Can. J. Chem.* **2001**, *79*, 1049−1057.

DOI: 10.1021/acsnano.8b01822
ACS Nano 2018, 12, 6714−6724